Structural properties of WO_3 dependent of the annealing temperature deposited by hot-filament metal oxide deposition

J. E. Flores-Mena
Facultad de Ciencias de la Electrónica, Benemérita Universidad Autónoma de Puebla,
Av. San Claudio y 18 Sur, Ciudad Universitaria, Colonia Jardines de San Manuel, 72570. Puebla, Pue., México.
email: eflores@ece.buap.mx

J. Díaz-Reyes
Centro de Investigación en Biotecnología Aplicada, Instituto Politécnico Nacional,
Ex-Hacienda de San Molino Km. 1.5. Tepetitla, Tlaxcala, 90700, México,
email: jdiazr2010@yahoo.com

J. A. Balderas-López
Unidad Profesional Interdisciplinaria de Biotecnología, Instituto Politécnico Nacional
Av. Acueducto S/N, Col. Barrio la Laguna, Delegación Gustavo A. Madero, México, D.F. 07340. México.

Recibido el 1 de agosto de 2012; aceptado el 7 de septiembre de 2012

In this work presents a study of the effect of the annealing temperature on structural and optical properties of WO_3 that has been grown by hot-filament metal oxide deposition (HFMOD). The chemical stoichiometry was determined by X-ray Photoelectron Spectroscopy (XPS). By X-ray diffraction obtained that the as-deposited WO_3 films present mainly monoclinic crystalline phase. WO_3 optical band gap energy can be varied from 2.92 to 3.15 eV obtained by transmittance measurements by annealing WO_3 from 100 to 500°C. The Raman spectrum of the as-deposited WO_3 film shows four intense peaks that are typical Raman peaks of crystalline WO_3 (m-phase) that corresponds to the stretching vibrations of the bridging oxygen that are assigned to W-O stretching (ν) and W-O bending (δ) modes, respectively, which enhanced and increased their intensity with the annealing temperature.

Keywords: Electrochromic semiconductor; WO_3; physical properties.

Este trabajo presenta un estudio del efecto de la temperatura de recocido sobre las propiedades ópticas y estructurales de WO_3 que ha sido crecido por deposición de óxido de metálico por filamento-caliente (HFMOD). La estequiometria química fue determinada por espectroscopia de fotoelectrones de rayos X (XPS). Por difracción de rayos X se obtuvo que las películas depositadas de WO_3 presentan principalmente fase cristalina monoclínica. La energía de la banda prohibida óptica del WO_3 puede ser variada desde 2.92 a 3.15 eV obtenidas por mediciones de transmitancia recociendo WO_3 desde de 100 a 500°C. El espectro Raman de la película depositada de WO_3 muestra cuatro picos intensos que son los picos típicos Raman de WO_3 cristalina (fase m) que corresponden a los modos de las vibraciones de estiramientos del puente de oxígeno que están asignados a estiramiento W-O (ν) y (δ) plegados de W-O, respectivamente, los cuales se magnifican e incrementa su intensidad con la temperatura de recocido.

Descriptores: Semiconductores electrocromicos; WO_3; propiedades fisicas.

PACS: 74.25.-q; 74.25.Gz; 74.25.nd; 78.70.Ck.

1. Introduction

Transition metal oxides represent a large family of materials possessing various interesting properties, such as superconductivity, colossal magneto-resistance and piezoelectricity. Among them, tungsten oxide is of great interest and has been investigated extensively for its distinctive properties. With outstanding electrochromic [1], photochromic [2], gaschromic [3], gas sensor [4], photo-catalyst [5] and photoluminescence properties [6], tungsten oxide has been used to construct "smart-window", anti-glare rear view mirrors for automobiles, non-emissive displays, optical recording devices, solid-state gas sensors, humidity and temperature sensors, biosensors, photonic crystals and so forth. WO_3 thin films can be prepared by various deposition techniques such as thermal evaporation [3,7], spray pyrolysis [8], sputtering [9], pulsed laser ablation [4], sol-gel coating [10] and chemical vapour deposition [11].

The purpose of this work is to characterize the WO_3 layers deposited by hot filament metal oxide deposition (HFMOD) technique, which were annealed in a wide temperature range. This growth technique has some advantage compared with the conventional growth technique, it is easily implemented and it is not expensive. The investigations so far carried out in the laboratory show that the films can be deposited with a good stoichiometric control, with relatively high deposition rates and present good adhesion to both metallic and dielectric substrates. The WO_3 thin films were characterized by X-ray Photoelectron Spectroscopy (XPS), X-ray scattering, transmittance measurements and Raman spectroscopy.

2. Experimental details

The WO_3 thin films were deposited by hot-filament metal oxide deposition (HFMOD) technique at atmospheric pressure

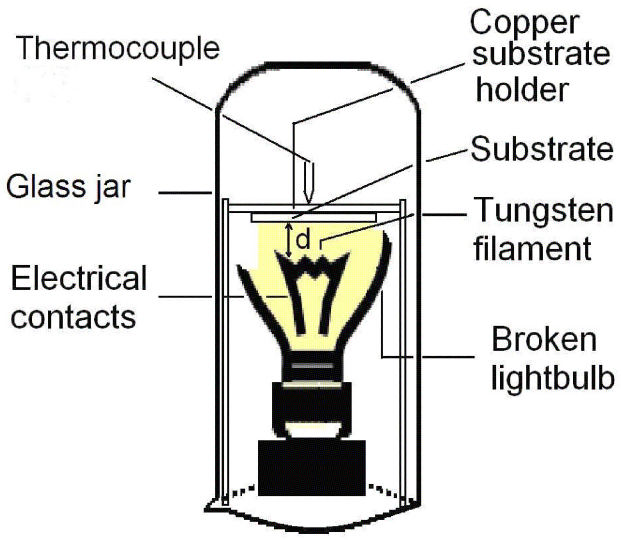

FIGURE 1. Experimental setting for the synthesis and deposition of WO_3 starting from a standard light bulb. Copper substrate holder of $50\times30\times7$ mm^3; thermocouple; filament-to-substrate separation: d = 30 mm.

and deposited on corning glass at room temperature. The details of the HFMOD growth system were published elsewhere [12]. Briefly, in Fig. 1 depicts the experimental deposition setup for the synthesis of transition metal oxides. The tungsten filament is obtained broking the outline of glass bulb to uncover it. Then it is connected to an AC power supply to induce its resistivity heating. Oxygen is introduced to the growth chamber via an electronic mass flowmeter. Pressure measurements are made using a capacitance manometer. The chamber base pressure is the atmospheric pressure.

For determining the WO_3 chemical stoichiometry was used X-ray Photoelectron Spectroscopy (XPS). For the XPS analyses, a hemispherical spectrometer using the unmonochromatized Kα X-ray line of aluminium was employed. To investigate the possible tungsten valence states, the 4f-doublet peak or the 3d-doublet peak, respectively, were fitted with Gaussian peaks corresponding to known bonding states of tungsten and oxygen atoms. The crystalline phase and structure was determined with a Bruker D8 Discover diffractometer using the copper K radiation (1.5406 Å) at 40 kV and 40 mA with parallel beam geometry. The transmittance spectroscopy analysis was performed using a Brucker Infrared Spectrometer Vertex 70. Raman scattering experiments were performed at room temperature using the 6328 Å line of a He-Ne laser at normal incidence for excitation. The laser light was focused to a diameter of 6.0 μm at the sample using a 50x (numerical aperture 0.9) microscope objective. The nominal laser power used in these measurements was 20 mW. Scattered light was analyzed using a micro-Raman system (Lambram model of Dilor), a holographic notch filter made by Kaiser Optical System, Inc. (model superNotch-Plus), a 256×1024-pixel CCD used as detector cooled to 140 K using liquid nitrogen, and two interchangeable gratings (600 and 1800 g/mm). Typical spectrum acquisition time was limited to 60 s to minimize the sample heating effects. Absolute spectral feature position calibration to better than 0.5 cm^{-1} was performed using the observed position of Si which is shifted by 521.2 cm^{-1} from the excitation line.

3. Results and discussion

Figure 2 shows the evolution of the W(4f) doublet peak of WO_3 deposited by HFMOD before and after 500°C treatment, here XPS is used to find the chemical stoichiometry and to confirm that the film is composed by WO_3. They have the same characteristics as bulk WO_3. Figure 2(a) shows the W(4f) core level spectrum recorded on the as-deposited WO_3 sample, and the results of its fitting analysis. In order to reproduce the experimental data, a doublet function was used for the W(4f) component. This contains W(4f$_{7/2}$) at 35.6 eV and W(4f$_{5/2}$) at 37.8 eV with a full-width at half-maximum (FWHM) of 1.75 ± 0.04 eV. The area ratio of these two peaks is ~ 0.75, which is supported by the spin-orbit splitting theory of 4f levels. Moreover, the structure was shifted by 5.0 eV towards higher energy relative to the metal state. It is thus clear that the main peaks in the typical XPS spectrum are attributed to the W^{6+} state on the surface [13,14], indicating that the deposited film is composed of stoichiometric WO_3. In stoichiometric WO_3, the six valence electrons of the tungsten atom are transferred into the oxygen p-like bands, which are thus completely filled. In this case, the tungsten 5d valence electrons have no part of their wave function near the tungsten atom and the remaining electrons in the tungsten atom experience a stronger Coulomb interaction with the nucleus than in the case of a tungsten atom in a metal, in which the screening of the nucleus has a component due to the 5d valence electrons. Therefore, the binding energy of the W(4f) level is larger in WO_3 than in metallic tungsten. If an oxygen vacancy exists, the electronic density near its adjacent tungsten atom increases, the screening of its nucleus is higher and, thus, the 4f level energy is expected to be at a lower binding energy [13]. After annealing at 400°C in nitrogen atmosphere all peaks in the spectrum had a slight shift in the direction of low energy. By increasing the annealing temperature, it was observed that the position of the W(4f) peak did not change appreciably up to temperatures lower than 400°C, which indicates that the films only improve their crystalline quality. But for WO_3 thin film annealed at 500°C, see Fig. 2, the W(4f) peak moved to a lower binding energy so that the W(4f$_{7/2}$) position was observed at 35.0 eV. This can be related to oxygen vacancies at this high annealing temperature and the formation of W^{5+}.

As-deposited WO_3 film presents mainly the monoclinic crystalline phase and a small fraction of orthorhombic crystalline phase that were obtained by X-ray diffraction and whose lattice parameters were calculated using the software DICVOL04, obtaining the following monoclinic lattice parameters values: a= 3.8465 Å, b= 7.5449 Å, c= 7.3066 Å, $\beta = 90.924°$ and its unit lattice volume is about 212.02 Å^3,

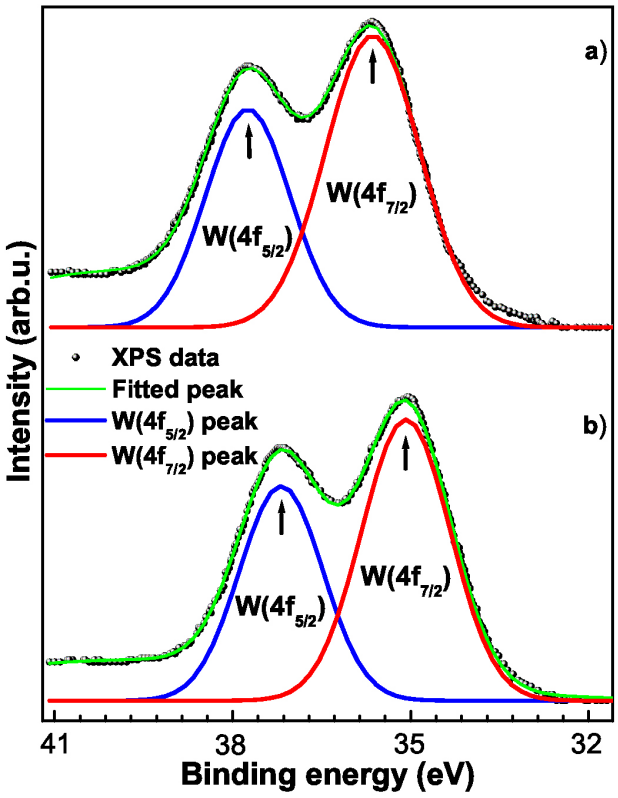

FIGURE 2. W(4f) core level spectra of WO_3 films: (a) as-deposited and (b) annealed at 500°C.

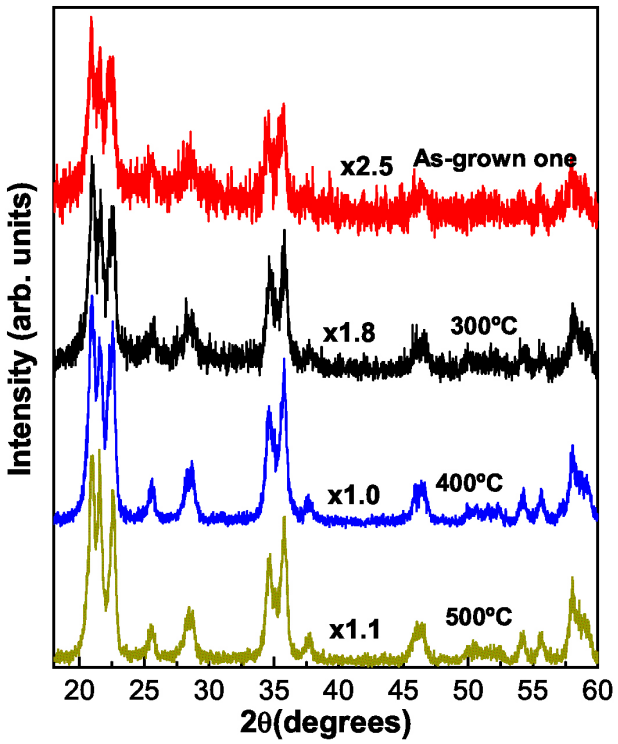

FIGURE 3. XRD diffractograms of WO_3 films deposited by heating resistive annealed at different temperatures. In each XRD diffractogram is indicated the intensities ratio related to the XRD pattern of the sample annealed at 400°C, $I_{TA}/I_{400°C}$.

further the X-ray patterns of the annealing WO_3 films are shown in Fig. 3. The XRD patterns obtained of the as-deposited sample and the annealed samples are quite similar, which indicates clearly that the WO_3 does not change of crystalline phase with the annealing in the investigated temperature range. As can see in Fig. 3, the intensity increases as the annealing temperature increases up to 400°C, in which the material has a better quality crystalline, and it undergoes a decrease of the intensity indicating a lower crystalline quality, as was found by XPS measurements due to the loss of oxygen by annealing one. As can observe in Fig. 3, each XRD diffractogram contains a factor that is its intensities ratio related to the XRD pattern of the sample annealed at 400°C ($I_{TA}/I_{400°C}$), which is more intense, for having a better reference of the one discussed above.

The transmittance spectra in the visible and infrared range are recorded for the WO_3 thin films before and after annealing at different temperatures in the energy range from 1.5 to 3.1 eV. Figure 4 shows the transmission spectra of WO_3 films prepared at room temperature, further heat treated in the temperature range from 100 to 500°C. The as-deposited tungsten oxide films were transparent, with no observable blue colouration under our experimental conditions. The transmittance of the WO_3 film annealed at 500°C is increased by about 10%, as can see in Fig. 4. The increase in transparency

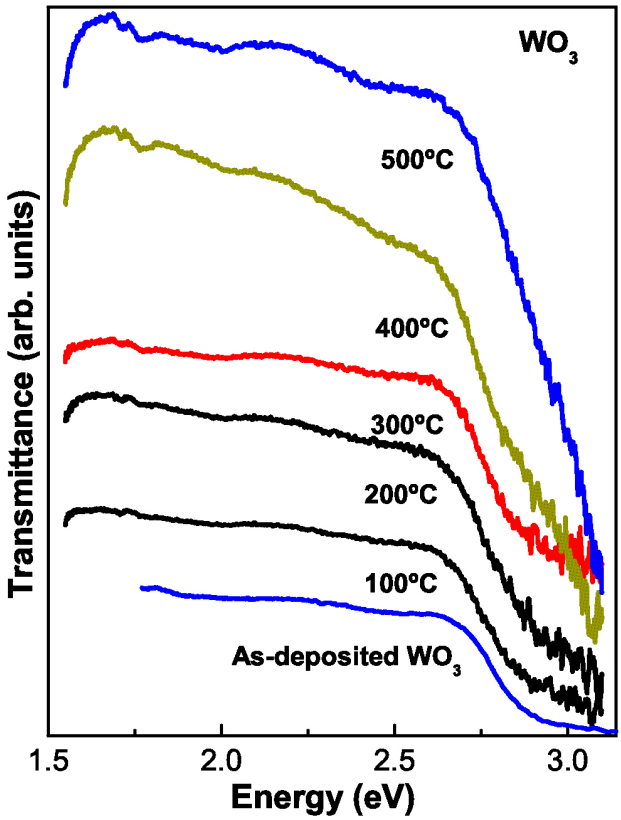

FIGURE 4. Optical transmittance of the WO_3 thin films deposited by HFMOD and annealed at different temperatures.

of the films with increased annealing temperature in nitrogen environment maybe due to the formation of more oxygen-ion vacancies in the films, the film changes to a non-stoichiometric composition, as could be seen from the change in colour of the film due to the excellent electrochromic nature. This causes the slight increase in energy band gap. It is observed from the transmittance spectra that the absorption edge is also slightly shifted towards the higher energy region for the films annealed at higher temperatures, owing to preferred colouration effect on the films. It confirms that the improvement in crystalline quality of the films increases with increasing annealing temperature, see Fig. 5.

The intrinsic absorption edge of the films can be evaluated and discussed in terms of the indirect interband transition. The optical band gap (E_G) was evaluated from the absorption coefficient α using the standard relation: $(\alpha h\nu)^{1/2} = A(h\nu - E_G)$. It is expected to show a linear behaviour in the higher energy region, which should correspond to a strong absorption near the absorption edge. Extrapolating the linear portion of this straight line to zero absorption edge gives the optical energy band gap of the films. The absorption coefficient α for a film of thickness d and reflectance R was determined near the absorption edge using the simple relation: $\alpha = \ln((1-R)^2/T + [((1-R^2)/2T)^2 + R^2]^{1/2})/d$, where multiple reflections are taken into, but interference neglected. Actually a transmission interference pattern could be observed in most samples, and was used to get an accurate value for the thickness d. The optical band gap for the as-deposited WO_3 is calculated about 2.92 eV, the polycrystalline structure of the as-deposited WO_3 could cause E_G to be bigger than 2.7 eV that correspond pure WO_3 indirect band gap in bulk [1]. In order to the sample annealed at 100°C, the optical band gap decreased slightly by about 20 meV, which can be related to condensation of the films. However, the optical band gap of the WO_3 annealed at range from 200 to 500°C is increased up to 3.15 eV due to recrystallization of the films. The reason E_G becomes bigger than

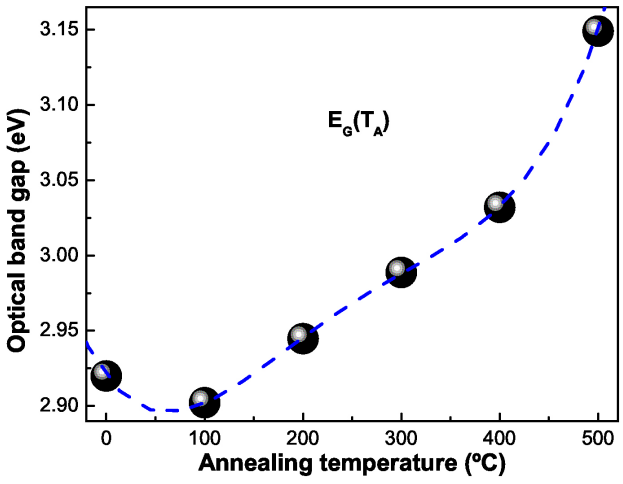

FIGURE 5. Optical band gap energy of the WO_3 thin films as-deposited and annealed at different temperatures.

2.7 eV is the creation of oxygen vacancy at these temperatures, as can see in Fig. 5. It is worth noting that has reported in the literature how for evaporated WO_3 films has found $2.7 < E_G < 3.5$ eV [1].

Figure 6 shows the Raman spectra of the samples studied in the work. The Raman spectrum of as-deposited WO_3 film shows mainly seven vibrational bands in range of 50-1000 cm^{-1} centered at 801, 710, 322, 262, 126, 81 and 65 cm^{-1}, see Figs. 6 and 7. As has been reported in the literature the WO_3 Raman bands sited in the range 750-950 cm^{-1} are attributed to either the antisymmetric stretch of M-O-M bonds (*i.e.*, ν_{as}[M-O-M]) or the symmetric stretch of (-O-M-O-) bonds (*i.e.*, ν_s[-O-M-O-]) [15]). Most peaks below 200 cm^{-1} are attributed to lattice vibrational modes, whereas the mid and high frequency regions correspond to deformation and stretching modes, respectively. Thus, the intense peaks centered at 801 and 710 cm^{-1} are typical Raman peaks of crystalline WO_3 (m-phase), which correspond to the stretching vibrations of the bridging oxygen [16,17] and these are assigned to W-O stretching (ν), W-O bending (δ) and O-W-O deformation (γ) modes, respectively [18,19]. In Fig. 7 illustrates the Raman spectrum in the range from 50 to 120 cm^{-1} for the as-deposited sample. It presents the typical characteristic peaks of the monoclinic crystalline phase at low frequencies that were obtained by deconvolution using Lorentzian curves for finding the peaks frequency, which are associated to lattice vibrational modes [20,21]. Similar vibration modes were obtained by Raman theories and are in agreement with the results of de Wijs *et al*. [17]. The sharp peaks at 262 and 322 cm^{-1} are assigned to the bending vibration δ(O-W-O) [18,20]. The Raman peak sited at 262 cm^{-1} is very intense, which means that a great fraction of crystalline phase is present in the as-deposited films. The peaks at 801, 710 and 262 cm^{-1} are very intense and typical modes of the crystalline WO_3 film. All these peaks are in good agreement with what has been published on WO_3 obtained by conventional techniques.

For corroborating the above discussed results, the WO_3 samples were annealed at different temperatures in the range from 0 to 500°C during 10 min in a nitrogen atmosphere. The Raman spectra of the samples annealed at 400 and 500°C are shown in Fig. 7. Before and after annealing the films show similar Raman curves [22]. Small variations of the intensity between the Raman spectra are found in all the range. All the background from the underlying glass slide in the spectra decreases after annealing at 300°C, that is, the IR/IN ratio of Raman intensity (IR) and noisy signal intensity (IN) increased after annealing. In particular, the Raman spectrum at low frequencies of the annealed sample at 500°C presents the same peaks that the spectrum of the as-deposited one and only the 65 cm^{-1} band is small and as the annealing temperature increases it becomes dominant displacing to higher frequencies. This fact corroborates that there is not change of crystalline phase. The Raman spectroscopy can give a clearer evidence of the crystalline evolution in function of the annealing temperature and allows following the different steps

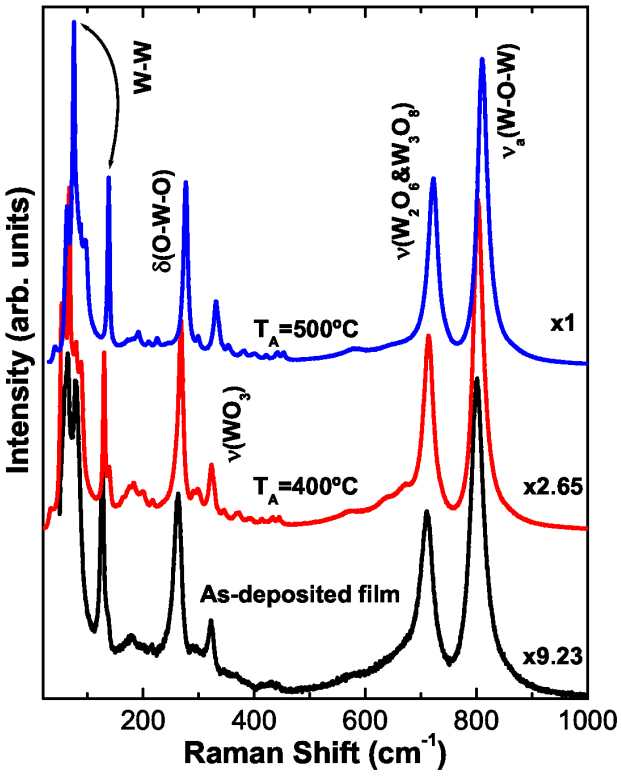

FIGURE 6. Raman spectra of WO_3 thin films annealed at different temperatures.

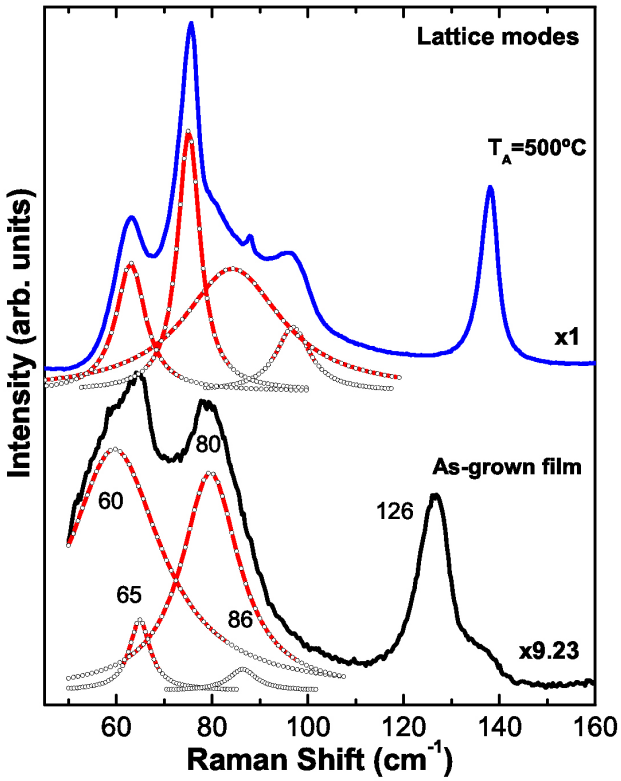

FIGURE 7. Raman spectra of two WO_3 thin films at low frequencies: as-deposited and annealed at 500°C.

if there is change of crystalline phase by analysing the evolution of lowest frequency peaks (up to 100 cm^{-1}) of the Raman spectra. These peaks correspond to lattice modes of vibrational nature and are noticeably affected by the transition between the low symmetry phases of WO_3. Most vibrational peaks below of 200 cm^{-1} in the WO_3 Raman spectrum are attributed to lattice modes [23]. As is observed in Fig. 7, only the Raman peaks are enhanced with the annealing, as is indicated by factor ($I_{TA}/I_{500°C}$) on each Raman spectrum.

All the above facts support the hypothesis of an open (or porous) structure of the films with many inner empty spaces and inter-grain boundaries. This means that comparably small amounts of water were absorbed in the films. The results suggest that the formation of porous films is due to gas-phase reactions in the plasma, leading to a homogeneous nucleation of oxide particles on the substrate. Clearly the prepared films were not a typical crystalline WO_3 (monoclinic phase or m-phase) structure. In addition probably an increase of compressive residual stress of the film due to annealing causes Raman shift to higher wavenumbers. This phenomenon has also been observed in IrO_2 films [24], ZrO_2 films [25] and on the GaAs-SiO_2 interface. Considering the residual stress and the Raman peak position before and after annealing, it can be concluded that the Raman peak position shifts to higher wavenumbers with the increase of compressive stress and it shifts to lower wavenumbers with the increase of tensile stress. To obtain a quantitative measurement of the residual stress of the WO_3 films, more detailed work is needed

4. Conclusions

In this work investigated the role of annealing temperature, as an external parameter, to control the optical and structural properties of WO_3 deposited by resistive heating. Using X-ray diffraction is obtained that WO_3 thin films only present as dominant phase the monoclinic and improved their structural quality with the annealing temperature up to 400°C and at higher temperatures occur the opposite case. By XPS measurements found that the as-deposited WO_3 is stoichiometric and that the annealing processes caused oxygen vacancies. The Raman spectroscopy indicates similar results, since the peak sited at 801 cm^{-1} shifted to 811 cm^{-1} when it is annealed at 500°C, this small change indicates a higher tungsten concentration than oxygen, which is indicative of a higher vacancy concentration. The highly transparent nature of the films has been observed from the optical transmittance spectra. The increase in transmittance with increasing annealing temperatures reveals the formation of oxygen vacancies in the films. The slight widening in the evaluated optical energy band gap values towards the increasing annealing temperature may be due to the optical band filling effect that reveals the crystallization of the films. One believes that these preliminary characteristic observations on the hot-filament metal oxide deposition WO_3 films will be helpful to explore the device performance of the films for electrochromic and smart window applications.

Acknowledgments

The authors are grateful for the financial support given by PROMEP-BUAP-CA-259 of Mexico. JEFM is grateful for the support given by VIEP-BUAP (project 31-ING-2012)

1. G. Granqvist, *Handbook of Electrochromic Materials* (Amsterdam: Elsevier, 1995).
2. C. O. Avellaneda and L. O. S. Bulhões, *Solid State Ionics* **165** (2003) 59-64.
3. S. H. Lee *et al*., *J. Appl. Phys*. **88** (2000) 3076-3078.
4. E. György, G. Socol, I. N. Mihailescu, C. Ducu and S. Ciuca, *J. Appl. Phys.* **97** (2005) 093527-093527-4.
5. M. A. Gondal, A. Hameed, Z. H. Yamani and A. Suwaiyan, *Chem. Phys Lett.* **385** (2004) 111-115.
6. M. Feng *et al*., *Appl. Phys Lett.* **86** (2005) 141901-141901-3.
7. R. Azimirad, O. Akhavan and A. Z. Moshfegh, *Journal of Electrochemical Society* **153** (2006) E11-E16.
8. J. Hao, S. A. Studenikin and M. Cocivera, *J. Appl. Phys.* **90** (2001) 5064-69.
9. Y. Takeda, N. Kato, T. Fukano, A. Takeichi and T. Motohiro, *J. Appl. Phys.* **96** (2004) 2417-2422.
10. G. Garcia-Belmonte, P. R. Bueno, F. Fabregat-Santiago and J. Bisquert, *J. Appl. Phys.* **96** (2004) 853-859.
11. M. Seman and C. A. Wolden, *Journal of Vacuum Science and Technology A* **21** (2003) 1927-1933.
12. J. Díaz-Reyes, V. Dorantes-García, A. Pérez-Benítez and J. A. Balderas-López, *Superficies y Vacío* **21** (2008) 12-17.
13. C. G. Granqvist, *In The CRC Handbook of Solid State Electrochemistry* P. J. Gellings, H. J. M. Bouwmesster, eds.; (CRC Press, Inc.: Cleveland Ohio, 1997, chapter. 16).
14. P. R. Bueno *et al*., *J. Appl. Phys* **96** (2004) 2102-2109.
15. M. F. Daniel, B. Desbat, J. C. Lassegues, and R. Garie, *Journal of Solid State Chemistry* **73** (1988) 127-139.
16. P. Tägtström and U. Jansson, *Thin Solid Films 352* (1999) 107-113.
17. G. A. de Wijs and R. A. de Groot, *Electrochimica Acta* **46** (2001) 1989-1993.
18. M. F. Daniel, B. Desbat, J. C. Lassegues, B. Gerand, and M. Figlarz, *Journal of Solid State Chemistry* **67** (1987) 235-247.
19. E. Salje, *Acta Crystallographic A.* **31** (1975) 360-363.
20. A. Rougier, F. Portemer, A. Quédé, and M. El Marssi, *Applied Surface Science* **153** (1999) 1-9.
21. M. Regragui *et al*., *Thin Solid Films* **358** (2000) 40-45.
22. J. V. Gabrusenoks, P. D. Cikmach, A.R. Lusis, J. J. Kleperis and G. M. Ramans, *Solid State Ionics* **14** (1984) 25-30.
23. D. Gazzoli, M. Valigi, R. Dragone, A. Marucci, and G. Mattei, *J. Phys Chem. B* **101** (1997) 11129-11131.
24. P. C. Liao, C. S. Chen, W. S. Ho, Y. S. Huang, and K. K. Tiong, *Thin Solid Films* **301** (1997) 7-11.
25. A. Portinha, V.Teixeira, J. Carneiro, M.F. Costa, N. P. Barradas, and A. D. Sequeira, *Surface and Coatings Technology* **188-189** (2004) 107-115.